Available online at www.sciencedirect.com
ScienceDirect
Journal of Power Sources 166 (2007) 537–548
JOURNAL OF POWER SOURCES
www.elsevier.com/locate/jpowsour

A model for the silver–zinc battery during high rates of discharge

Murali Venkatraman, J.W. Van Zee *

Department of Chemical Engineering, University of South Carolina, Columbia, SC 29208, United States

Received 3 October 2006; received in revised form 13 December 2006; accepted 14 December 2006
Available online 12 January 2007

Abstract

A transient one-dimensional mathematical model is developed and used to study the performance and thermal behavior of the silver–zinc cell during discharge. The model considers the negative (zinc) electrode, separator, and positive (silver) electrode and describes the simultaneous electrochemical reactions in the positive electrode, mass transfer limitations, and heat generation. Changes in porosity and electrolyte composition due to electrochemical reactions, local reaction rates, diffusion, and migration of electrolyte are reported. Emphasis is placed on understanding the movement of the reaction front in the negative electrode during discharge and its correlation to the useful capacity of the cell. The sensitivity of this capacity to changes in the values of initial electrolyte, exchange current densities, and tortuosity are presented. It is shown that under certain conditions, in a system employing 25% KOH as the electrolyte, the useful capacity of the cell could be limited to 55.6% of its rated capacity when the discharge rate is increased from 1*C* to 2*C*. The temperature rise in a single cell was predicted and observed to agree with the experimental values.

Keywords: Silver–zinc battery; Model; Constant current discharge; Porous electrodes; Multiple electrode reactions

1. Introduction

Even though the silver–zinc battery has a high cost, it is one of the more important secondary batteries available today because of its high discharge rate capability and because of its large specific energy density on both a mass and a volumetric basis [1]. As discussed below, the shape change effects have limited the robustness of this rechargeable system. The most important characteristic of this battery is that initially the impedance is very low but it can vary considerably with factors such as discharge current density, state-of-discharge, operational temperature, active material composition, cell ageing, and cell size [2]. It is rechargeable with little overcharge but it has low cycle life primarily resulting from zinc-electrode shape change. The calendar life is also short due to the degradation of the separator in alkaline conditions, but new separator materials have been developed to offer stability [3]. A physical description of the silver–zinc battery, with design specifications and calculations, has been provided by Himy [4]. A wealth of experimental information is available on the behavior of silver–zinc cells [5–10], but models that describe these cells are scarce in literature and have been focused on only part of the cell as discussed later. As a first step towards understanding the behavior of a rechargeable Ag–Zn battery during cycles, we present here a time-dependent one-dimensional model to explain the distribution of reactants and the thermal behavior of a silver–zinc cell during high rates of discharge. This discharge behavior at high rates establishes a basis for future analyses of the recharge behavior which requires initial conditions corresponding to the end of discharge concentration and temperature profiles, and which is performed at much slower rates due to chemical complexities of the system (including zinc-electrode shape change mechanisms) not important during discharge.

The first reproducible and stable silver-silver oxide electrode was prepared by Hamer and Craig [11,12]. Dirkse [13] has extensively reviewed the electrochemistry of the silver electrode. Wales and Burbank [14,15] conducted galvanostatic and potentiostatic studies along with X-ray diffraction. They concluded from their X-ray diffraction patterns that the major components of a silver electrode are Ag, AgO, and Ag_2O. No higher oxide could be observed. Dirkse [16] showed that the OCVs of silver–zinc cells in the neighborhood of 1.66 V correspond to the presence of $Ag/Ag_2O/OH^-$ system in the silver electrode, and those near 1.93 V correspond to $AgO/Ag_2O/OH^-$ system.

* Corresponding author. Tel.: +1 803 777 7555; fax: +1 803 777 8142.
E-mail address: vanzee@engr.sc.edu (J.W. Van Zee).

0378-7753/$ – see front matter © 2007 Elsevier B.V. All rights reserved.
doi:10.1016/j.jpowsour.2006.12.064

Nomenclature

a_{Ag}	specific surface area of silver electrode
a_{Zn}	specific surface area of zinc electrode
$c_{p,i}$	specific heat capacity of species i ($J\,K^{-1}\,kg^{-1}$)
C	concentration of OH^- ions ($kmol\,m^{-3}$)
C_{ref}	reference concentration of OH^- ions ($kmol\,m^{-3}$)
C_0	initial concentration of OH^- ions ($kmol\,m^{-3}$)
D	diffusivity of KOH ($m^2\,s^{-1}$)
D_i	diffusivity of species i ($m^2\,s^{-1}$)
F	Faraday's constant (96,487 C)
i_{nj}	transfer current of the jth reaction the silver electrode ($A\,m^{-2}$)
i_1	matrix current density ($A\,m^{-2}$)
i_2	solution current density ($A\,m^{-2}$)
i_{0j}	equilibrium exchange current density for jth reaction ($A\,m^{-2}$)
k_i	thermal conductivity of species i ($W\,m^{-1}\,K^{-1}$)
m_i	mass fraction of species i on an electrolyte free basis
M_i	molar density of species i ($kmol\,m^{-3}$)
M_i^w	molecular weight of species i ($kg\,kmol^{-1}$)
n_j	number of electrons transferred in reaction j
N_i	flux of species i ($mol\,m^{-2}\,s^{-1}$)
Q	total heat source term in energy equation ($J\,m^{-3}\,s^{-1}$)
Q_{kin}	kinetic heat source term in energy equation ($J\,m^{-3}\,s^{-1}$)
Q_{ohm}	joule heating term in energy equation ($J\,m^{-3}\,s^{-1}$)
R	universal gas constant, 8.314 ($J\,mol^{-1}\,K^{-1}$)
$S_{a,i}$	stoichiometric coefficient of species 'a' in ith reaction
t	time (s)
T	temperature (K)
T_0	initial temperature (K)
U_j^θ	equilibrium potential of jth electrochemical reaction (V)
V_{Ag}	volume of silver electrode
V_{Zn}	volume of zinc electrode
w_i	mass fraction of species i (electrolyte included)
Z_i	charge of species i

Greek letters

α_{ai}	anodic transfer coefficient for reaction i
α_{ci}	cathodic transfer coefficient for reaction i
ε_r	porosity of region r
η_j	overpotential for jth reaction (V)
θ_1	initial mass ratio of zinc to silver in the cell
θ_2	initial mass ratio of silver in Ag_2O to silver in AgO
κ_r	conductivity of region r ($mho\,m^{-1}$)
ρ_i	density of species i ($kg\,m^{-3}$)
σ_i	electrical conductivity of the species i ($mho\,m^{-1}$)
ϕ_1	matrix potential (V)
ϕ_2	solution potential (V)
∇	differential operator

Intermediate potentials are mixed potentials due to the presence of all the three. Gagnon and Austin [17] have examined the discharge mechanism of a porous silver-oxide electrode at low temperature in a KOH electrolyte.

The zinc electrode is one of the most researched electrodes in the literature since it forms the anode for many battery systems, such as the Ag–Zn, Zn–Br_2, Zn–MnO_2 (i.e., alkaline zinc) and the zinc-air and a comprehensive listing of the relevant literature has been provided by McLarnon and Cairns [18]. Most of the literature on zinc electrodes focuses on the shape change effects, and this is relevant for the Ag–Zn battery since, aside from initial material costs, the shape changes are the major difficulty in recharging this battery and therefore limit its cycle life, ubiquitous use, and cost/cycle. Choi et al. [19,20] were among the first to analyze the shape change effect that is associated with zinc electrode. Shape change, the redistribution of active material over the zinc electrode surface as a result of cell cycling, was hypothesized to be caused by convective flows driven primarily by membrane pumping. They proposed a model and showed that shape change can be eliminated if the convective flow in the zinc electrode compartment parallel to the electrode surface is stopped. Hamby and Wirkkala [21] also have shown deformation of zinc electrode during oxidation. Theoretical [22] and experimental [23] work on transient and failure analyses was done by Sunu and Bennion, who reported that the depletion of electrolyte was the major cause of incomplete discharge in zinc electrode. Skelton and Serenyi [24] have discussed the use of BiO_2 as an additive to the zinc electrode to prevent the deleterious effects of shape change which lead to loss of active material during cycling. Cheh's group has also treated the Zn anode as part of their nine papers on the alkaline-zinc cell [25].

The model presented in this paper is based on porous electrode theory [26,27] follows the isothermal single cell model of Blanton et al. [28], is based on the literature for the prediction of the thermal behavior of batteries [29–35] and it features a typical silver–zinc cell whose specifications are based in Ref. [4] and on the advice of Moden [36]. The results are consistent with Moden's extensive experience with these batteries and his transient lumped-parameter spreadsheet model which captures changes in the cell voltage and cell temperature rise that are consistent with his experiments.

2. Model

The schematic of a silver–zinc cell is given in Fig. 1. It features a cathode made of silver–silver(I) oxide–silver(II) oxide (Ag–Ag_2O–AgO) supported by a silver grid. The silver grid serves as a current collector and it is non-reactive, typically. The separator material used is a combination of nylon, cellophane and FRSC, with a wrap of each material one above the other forming a three-layer structure. For modeling purposes, the separator is considered a single entity with average properties. The anode is made of zinc–zinc oxide (Zn–ZnO). The anode, separator and cathode are porous. Himy [4] provides a description of the preparation of the two electrodes observing that it is difficult to achieve reproducibility in case of zinc electrode preparation.

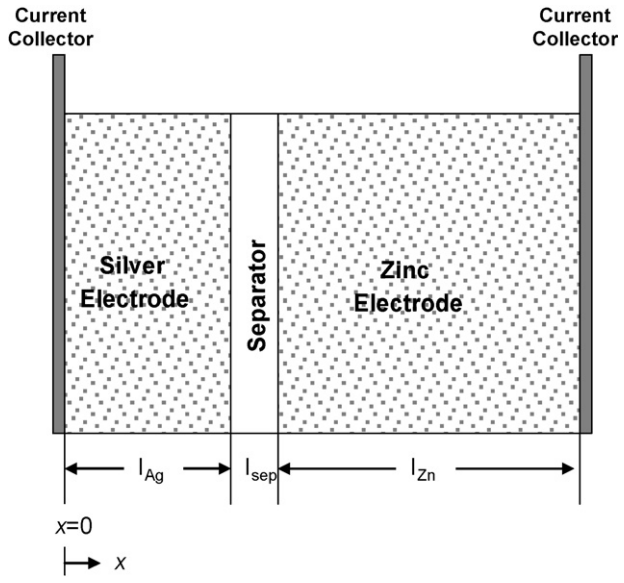

Fig. 1. Schematic representation of a silver–zinc cell. All the regions except the current collectors are porous and filled with KOH solution as the electrolyte. For the results presented here $l_{Ag} = 0.1067$ cm, $l_{sep} = 0.05$ cm, and $l_{Zn} = 0.4$ cm.

On discharge, the following reactions are assumed to occur at the cathode:

$$Ag_2O + H_2O + 2e^- = 2Ag + 2OH^-, \quad U_1^\theta = 0.604\,V \tag{1}$$

$$2AgO + H_2O + 2e^- = Ag_2O + 2OH^-, \quad U_1^\theta = 0.604\,V \tag{2}$$

and at the anode:

$$Zn + 2OH^- = ZnO + H_2O + 2e^-, \quad U_3^\theta = -1.305\,V \tag{3}$$

The zinc electrode operates according to a dissolution–precipitation reaction mechanism. The reaction mechanism is as follows:

$$Zn + 4OH^- \rightleftarrows Zn(OH)_4{}^{2-} + 2e^- \tag{4}$$

$$Zn(OH)_4{}^{2-} \rightleftarrows ZnO + 2OH^- + H_2O, \quad K_{eq} = 2.32 \times 10^{-2} \tag{5}$$

Although the model presented here is concerned with discharge limitations during a single cycle and thus shape change effects due to ZnO precipitation are not considered, a brief discussion will yield a useful perspective. During discharge, zinc is oxidized to soluble zincate $Zn(OH)_4{}^{2-}$, which is precipitated as ZnO when the solubility limit of zinc oxide is exceeded. Problems associated with these solid particles of ZnO are manifold because they affect not only the shape of the electrode (in the plane perpendicular to that shown in Fig. 1), but also the thermal and electrical conductivities adversely. Their high specific gravity causes an uneven distribution of precipitated ZnO and results in non-uniform current distribution which affects the ability to charge the cell uniformly. Also, during discharge, the concentration of OH^-, decreases in the anode and increases in the cathode and limits the discharge capacity and the solubility of Zn. For this discharge model we consider that the solution is saturated with $Zn(OH)_4{}^{2-}$ at a concentration which is much lower than the alkali concentration and thus use reaction (3) rather than reactions (4) and (5). However, we do assume that ZnO precipitation alters the porosity, thermal and electrical conductivities.

In a silver–zinc cell, the conductivities of the materials involved are very high and thus to a first approximation, a sandwich or one-dimensional model on the thickness is adequate. Then we use Newman's macro-homogenous model of porous electrodes along with the constitutive laws of a binary dilute solution [37], to predict the profiles of various variables. The complete set of equations can be found in [38] and those tables have been omitted for brevity here. As an overview, a material balance for species i in the solution phase is given by:

$$\frac{\partial(\varepsilon C_i)}{\partial t} = a j_{in} - \nabla \cdot N_i \tag{6}$$

where N_i is the flux of species i in the pore solution averaged over the cross sectional area of the electrode and aj_{in} represents the transfer rate of species i from the solid phases to the pore solution per unit electrode volume. The electrolyte is highly concentrated in K^+ and OH^-, relative to the zincate ion and hence the zincate ion's contribution is neglected and the solution is treated as a binary electrolyte of K^+ and OH^-. This is also consistent with the assumption of using only reaction (3) at the anode. Any convection inside the cell is considered negligible due mainly to the tight packing and hence only the diffusion and migration fluxes contribute to the movement of species in the cell. Hence, the respective flux equations are:

$$N_{K^+} = -\frac{\varepsilon}{\tau}\left(D_{K^+}\nabla C_{K^+} - \frac{D_{K^+}Fz_{K^+}C_{K^+}}{RT}\nabla\phi_2\right) \tag{7}$$

$$N_{OH^-} = -\frac{\varepsilon}{\tau}\left(D_{OH^-}\nabla C_{OH^-} - \frac{D_{OH^-}Fz_{OH^-}C_{OH^-}}{RT}\nabla\phi_2\right) \tag{8}$$

The binary electrolyte approximation along with electroneutrality yields:

$$C_{K^+} = C_{OH^-} = C \tag{9}$$

This leads to a single concentration equation devoid of the potential term:

$$\frac{\partial(\varepsilon C)}{\partial t} = -\nabla \cdot \left(-\frac{\varepsilon}{\tau}D\nabla C\right) + \left(\frac{D}{2D_{OH^-}}\right) a j_{in} \tag{10}$$

where

$$D = \frac{2D_{K^+}D_{OH^-}}{D_{K^+} + D_{OH^-}} \tag{11}$$

Note that, we have used the dilute binary electrolyte theory [37] in the formulation of the above equations. These equations are consistent with those formulated from concentrated solution theory [27] equations because in the Ag–Zn system the partial molar volume of the electrolyte and the transference number of

Table 1
Transport and electrode parameters (references in braces)

Parameter	Value	Source
a_{Ag}	$50\,m^{-1}$	Assumed
a_{Zn}	$50\,m^{-1}$	[42]
D_{OH^-}	5.26×10^{-9} ($m^2\,s^{-1}$)	[37] (p. 55)
D_{K^+}	1.96×10^{-9} ($m^2\,s^{-1}$)	[37] (p. 55)
n_1	2	Reaction (1)
n_2	2	Reaction (2)
n_3	2	Reaction (3)
$s_{OH^-,1}$	2	Reaction (1)
$s_{OH^-,2}$	2	Reaction (2)
$s_{OH^-,3}$	2	Reaction (3)
$s_{Ag,1}$	2	Reaction (1)
$s_{AgO,2}$	−2	Reaction (2)
$s_{Ag_2O,1}$	−1	Reaction (1)
$s_{Ag_2O,2}$	1	Reaction (2)
$s_{Zn,3}$	2	Reaction (3)
V_{Ag}	$7.3 \times 10^{-6}\,m^3$	[36]
V_{Zn}	$27.5 \times 10^{-6}\,m^3$	[36]
z_{K^+}	1	–
z_{OH^-}	−1	–
α_{a1}	0.65	Assumed
α_{c1}	0.35	Assumed
α_{a2}	0.75	Assumed
α_{c2}	0.25	Assumed
α_{a3}	0.5	[42]
α_{c3}	0.5	[42]
ε^0_{Ag}	0.322	[36]
ε_{sep}	0.5	[36]
ε^0_{Zn}	0.731	[36]
θ_1	0.866	[36]
θ_2	0.333	[36]
ξ	1.5	[29]

the cation (K^+) do not change with concentration. These approximations are consistent with the parameters and concentrated solution model of Chen and Cheh [25]. Also, D was found to be a constant for the range of concentrations employed in this study (see Table 1) and therefore the spatial variation of transference number of the solvent is also 0 [27].

In case of solid species, the mass balance does not involve a flux term. Thus, Eq. (6) simplifies as:

$$\frac{\partial M_k}{\partial t} = a j_{in} \tag{12}$$

where M_k is the molar density of the solid species k. In case of silver–zinc cell, the products and reactants are solids. Hence, an overall mass balance on the solid phases in each individual electrode is applicable:

$$\text{cathode}: \quad 2M_{Ag_2O} + M_{AgO} + M_{Ag} = M^{tot}_{Ag} \tag{13}$$

$$\text{anode}: \quad M_{ZnO} + M_{Zn} = M^{tot}_{Zn} \tag{14}$$

In addition, the superficial current density in the pore solution is due to the movement of the ions:

$$i_2 = F \sum z_i N_i = -\kappa \nabla \phi_2 - \varepsilon F (D_{K^+} - D_{OH^-}) \nabla C \tag{15}$$

where

$$\kappa = \frac{\varepsilon F^2}{RT} \sum z_i^2 D_i C_i = \frac{\varepsilon F^2}{RT} (D_{K^+} D_{OH^-}) C \tag{16}$$

The second term in the RHS is the diffusion potential term which would vanish for $D_{K^+} = D_{OH^-}$. However, our model uses different values for D_{K^+} and D_{OH^-}. The charge conservation equation for the matrix and solution phases would require the divergence of the total current to be 0:

$$\nabla \cdot i_1 + \nabla \cdot i_2 = 0 \tag{17}$$

For j simultaneous reactions of the form:

$$\sum_i s_{ij} X_i^{z_i} \rightarrow n_j e^- \tag{18}$$

Faraday's law can be expressed as:

$$a j_{in} = -\sum_j \frac{s_{ij}}{n_j F} a i_{nj} \tag{19}$$

The transfer current per unit electrode volume $\nabla \cdot i_2$ is related to the individual average transfer current densities by:

$$\nabla \cdot i_2 = \sum_j a i_{nj} \tag{20}$$

The movement of electrons in the matrix phase is governed by Ohm's law:

$$i_1 = -\sigma_{avg} \nabla \Phi_1 \tag{21}$$

where σ_{avg} is the effective electrical conductivity of the matrix and ϕ_1 is the potential in the matrix. The effective electrical conductivity of the matrix is obtained by considering parallel conduction paths and is given as:

$$\sigma_{avg} = \sum \sigma_k m_k^{\xi} \tag{22}$$

where m_k is the mass fraction (defined over solid phase only) of the solid species k and ξ being an empirical constant. A value of 1.5 was taken for ξ, as has been conventional in the literature [29].

Polarization equations are needed to express the dependence of the local rate of each reaction on the various concentrations and on the potential difference driving force at the reaction interface. In case of silver–zinc cells, since all the products and reactants except OH^- are solids, appropriate *capacity correction factors* must be used in the Butler–Volmer expressions so that the polarization equations take the form:

$$i_{nj} = i_{0j,ref} \left(\prod_i \left(\frac{C_i}{C_{i,ref}} \right)^{p_i} \prod_k \left(\frac{M_k}{M_{k,ref}} \right)^{p_k} \exp\left(\frac{\alpha_{aj} n_j F}{RT} (\varphi_1 - \varphi_2 - U_{j,ref}) \right) - \prod_i \left(\frac{C_i}{C_{i,ref}}^{q_i} \right) \prod_k \left(\frac{M_k}{M_{k,ref}} \right)^{q_k} \exp\left(\frac{-\alpha_{cj} n_j F}{RT} (\varphi_1 - \varphi_2 - U_{j,ref}) \right) \right) \tag{23}$$

Table 2
Densities and thermal parameters (references in braces)

Material	Parameter			
	c_p (J K^{-1} kg^{-1})	σ (mho m^{-1})	k (W m^{-1} K^{-1})	M^0 (kmol m^{-3})
Ag	234 [43]	6.28×10^7 [13]	430 [43]	0.0 [36]
AgO	343 [36]	8.33×10^4 [13]	20.7 [43]	3.0 [36]
Ag_2O	343 [36]	10^{-6} [13]	20.7 [43]	0.5 [36]
Electrolyte (KOH)	2520 [36]	–	2.0 [4]	See Table 3, for value of C_0
Cellophane separator	1340 [36]	0 (assumed)	0.24 [43]	–
Zn	389 [36]	1.83×10^7 [42]	120 [43]	1.5 [36]
ZnO	2910 [36]	1.0 [42]	20.7 [43]	0.0 [36]

For the silver and zinc electrodes the capacity correction factors $M_k/M_{k,\mathrm{ref}}$ are obtained by normalizing the molar densities of solid species against the total silver and zinc content of the electrodes, respectively. Similar expressions for silver electrode have been reported in literature [28].

The porosity equation is obtained calculating the volume change in the electrode as the discharge progresses:

$$\frac{\partial \varepsilon}{\partial t} = \left(\sum_{\text{solid phases}} \sum_{k} \frac{s_k M_k^{\mathrm{w}}}{\rho_k n F} \nabla \cdot i_2 \right) \tag{24}$$

The energy equation may be written as:

$$(\rho c_p)_{\mathrm{avg}} \frac{\partial T}{\partial t} = -\nabla \cdot (k_{\mathrm{avg}} \cdot \nabla T) + Q \tag{25}$$

In the above equation, ρ, c_p and k_{avg} are instantaneous values averaged on the composite material:

$$(\rho c_p)_{\mathrm{avg}} = c_{p,\mathrm{l}} \rho_{\mathrm{l}} \varepsilon + (1-\varepsilon) \sum c_{p,\mathrm{s}} \rho_{\mathrm{s}} M_{\mathrm{s}}^{\mathrm{w}} M_{\mathrm{s}} \tag{26}$$

$$k_{\mathrm{avg}} = \sum_{\text{all solids}} k_{\mathrm{s}} [(1-\varepsilon) w_{\mathrm{s}}]^{\xi} + \sum_{\text{all liquids}} k_{\mathrm{l}} [\varepsilon w_{\mathrm{l}}]^{\xi} \tag{27}$$

where s denotes the solid phase and l denotes the electrolyte. The source term Q, comprises of the heating from ohmic and kinetic phenomena. In a half-cell a part of the reaction enthalpy goes to heat up the system and the rest goes out as the electric power of the system [39]. The source term in the energy balance can be written [32]:

$$Q = \sum_j a i_j \left(\eta_j - T \frac{\partial U_{j,\mathrm{ref}}}{\partial T} \right) + \left(\frac{i_1 \times i_1}{\sigma_{\mathrm{avg}}} + \frac{i_2 \times i_2}{\kappa} \right) \tag{28}$$

Numerical solution of the system of equations was obtained through the finite element software FEMLAB [40] (version 2.1). The FEMLAB engine is designed to solve a set of coupled differential–algebraic equations of second order. The convergence criterion was that the difference between two successive solutions at all mesh points be less than 10^{-5} (relative tolerance) for all variables.

3. Results and discussion

An important capability of a battery model is the ability to predict the dependence of cell voltage on state of discharge (SOD) and the maximum state of discharge (MSOD) beyond which the voltage is so low at a fixed current that battery stops discharging. Depending on the rate of discharge the MSOD may not be equal to the capacity and it is the purpose of this paper to explain this behavior in the silver–zinc cell. In this section, we present the effects of various parameters on the discharge characteristics of the silver–zinc cell, transient electrolyte concentration distributions, the reaction rate and current density profiles, porosity variations and predicted temperature rise in the cell during discharge. The values for the parameters are listed in Tables 1–3 and also in the nomenclature where appropriate. Note that the literature is devoid of many of the critical parameters required by the model and that these tables are consistent with the data from Refs. [4,36,41].

Table 3
Perturbed parameters (references for base case values in braces)

Parameter	Figure number	Curve number	Value
T_0	All	All	298 K
C_0	2, 12	1, 4	45% KOH
	2, 12	2, 5	35% KOH
	2, 12	3, 6	25% KOH [36]
	3, 5–11, 13	All	25% KOH [36]
	4	All	45% KOH
$\tau_{\mathrm{Ag}} = \tau_{\mathrm{sep}} = \tau_{\mathrm{Zn}}$	4	1, 4	1.0
	4	2, 5	2.0
	4	3, 6	3.0
	2, 3, 5–13	All	1.0
i_{01}	1–9, 11, 12	All	2×10^{-3} A cm^{-2}
	10, 13	1, 4	2×10^{-3} A cm^{-2}
	10, 13	2, 5	2×10^{-4} A cm^{-2}
	10, 13	3, 6	2×10^{-5} A cm^{-2}
i_{03}	1–9, 11, 12	All	1.75×10^{-3} A cm^{-2} [18]
	10, 13	7, 9	1.75×10^{-2} A cm^{-2}
	10, 13	8, 10	1.75×10^{-3} A cm^{-2}

The 1C and 2C[1] rates of discharge for the silver–zinc cell under study correspond to 0.36 A (0.02 A cm^{-2}) and 0.71 A (0.04 A cm^{-2}), respectively. These rates were chosen to illustrate the limitations for moderate to high discharge rates with the parameters of Tables 1–3.

[1] A 1C rate is the current required to charge or discharge the cell in 1 h (as calculated based on the limiting reactant).

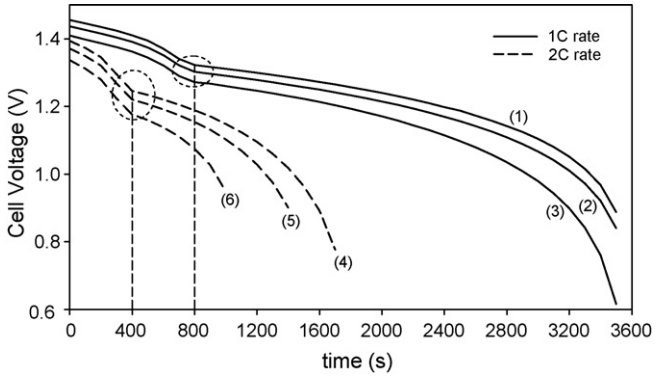

Fig. 2. Effect of initial concentration (%KOH) on cell voltage. For curves (1)–(6), see Table 3, for the parameter values. The encircled regions indicate the change in the behavior of the the silver electrode at $t = 800$ and 400 s for 1C and 2C rate discharges, respectively. The solid and dashed lines correspond to 1C and 2C, respectively.

3.1. Effect of initial and transient electrolyte compositions

As a baseline for future studies of transient cycles, the dependence of the discharge characteristics of the cell on the initial electrolyte concentration, C_0, is illustrated in Fig. 2, for 1C and 2C rates with the other parameters held constant. The solid lines correspond to 1C rate and the dotted lines correspond to 2C rate discharges. Three values of C_0: 25, 35, and 45% KOH were studied and help quantify that the cell-voltage increases by approximately 0.02 V for every 10% rise in initial KOH concentration. The MSOD for 1C rate is approximately 94% irrespective of C_0 but C_0 strongly affects the capacity utilization at 2C. The curves 4–6 in Fig. 2 illustrate that with 25, 35, and 45% KOH, the MSOD is 55.6, 77.7, and 94.4%, respectively, for a 2C rate discharge (i.e., 1000, 1400, and 1700 s, respectively). This is because, at 1C rate discharge, the rate of diffusion is comparable to the rate of OH^- production but at a 2C rate, the diffusion process is not fast enough to replenish and compensate the continuous consumption of OH^- in the negative electrode during discharge. Consequently this leads to a faster local depletion of OH^- ions in the anode and stops the cell from discharging further, leading to low capacity utilization and hence a low value of MSOD. However, when a higher concentration of KOH is used, the amount of OH^- ions available increases leading to a higher MSOD. The circled regions show the changes in the electrochemical phenomena for silver electrode as discussed below.

The initial OH^- concentration affects the SOD because the rate of transport of OH^- from the positive to the zinc electrode limits the battery. This limitation is best shown with the transient concentration profiles of OH^- ions for 1C and 2C rates. In Fig. 3, the solid lines show the extremes, namely 0% SOD and MSOD. The dotted lines show the variation of the profile of C across the cell in the x direction at various times. Thus, even though there is available Zn, the changes in the local concentration directly influence the extent of local utilization of the active material and hence the Nernst relationship for the cell potential. At high rates of discharge, the rate of consumption of OH^- ions is not matched by the diffusion and hence a concentration profile develops and diffusion aids migration. A linear concentration gradient is established across the separator that corresponds to the flux of the OH^- ions needed for the specified current density. This suggests that a reservoir if placed at the separator–cathode interface, could attenuate the local depletion of OH^- ions thereby ensuring a greater depth of discharge or higher active mass utilization. Fig. 3 also shows that higher the discharge rate higher the concentration of OH^- ions in the silver electrode and lower in the zinc electrode. In other words the difference between the average concentrations of both the electrodes is higher for a higher discharge rate.

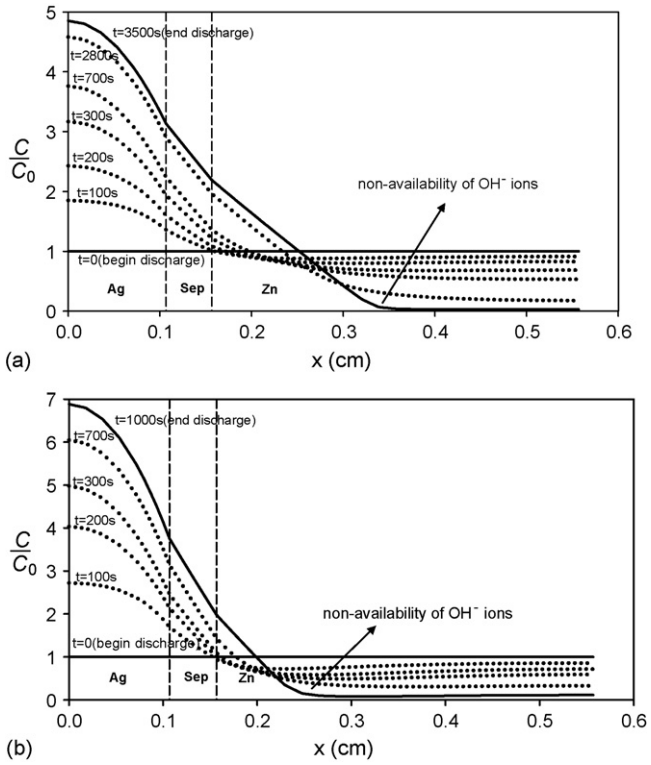

Fig. 3. Concentration profiles of OH^- ion during discharge at various times for (a) 1C rate and (b) 2C rate, respectively. Note that the local concentration of OH^- goes to 0 at 0.34 and 0.25 cm for 1C and 2C rates, respectively.

3.2. Effect of tortuosity (τ)

The transport rates could be changed by adjusting the tortuosity of the materials in the cell since these adjust the diffusion coefficient directly. Fig. 4 shows the discharge curves for 1C and 2C rates for three values of τ. See Table 3, for the values of parameters that correspond to the curves. An increase in tortuosity corresponds to a increased path length for diffusion which decreases the effective diffusivity. This reduction in diffusivity leads to a faster local depletion of the OH^- ions thus decreasing the MSOD considerably. Unlike C_0, τ has a considerable influence in the low rates (1C) also. Curves 1, 2, and 3 show MSOD values 97.2, 94.4, and 88.8%, respectively, for 1C rate discharge as τ is increased from 1.0 to 2.0 and then to 3.0. For the 2C rate the curves 4, 5, and 6 show MSOD values 94.4, 61.1, and 38.9%, respectively. Thus, at higher rates, the larger tortuosity leads to

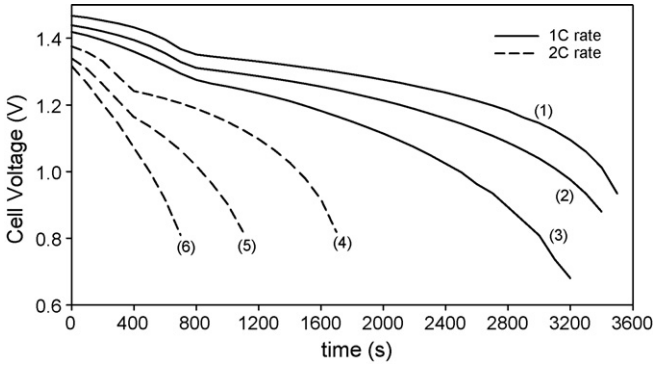

Fig. 4. Effect of tortuosity (τ) on cell performance. For curves (1)–(6), see Table 3, for the parameter values.

considerably low capacity utilization. The effects of C_0 and τ suggest that if a silver–zinc cell be subjected to high discharge rates from an incompletely charged battery, the concentration of KOH be made sufficiently high, to ensure maximum utilization of capacity. However beyond a certain concentration, the diffusion coefficients may show a very strong dependence on the concentration [42] and may decrease with an increase in concentration. A higher temperature of operation may be used in such a case. Before we present the effects of changes in the kinetic parameters such as the exchange current densities, it is important to understand the reaction distribution in both the electrodes.

3.3. Reaction profiles

3.3.1. Zinc electrode

Fig. 5 shows the fraction of active material unutilized within the zinc electrode, at several discharge times for 1*C* and 2*C* rates. At 1000 s for 1*C* there is 31% of the original Zn available at the separator (i.e., $x = 0.1567$ cm). This fraction is 0 at 2000 s at the separator and the position at which this zero fraction moves to is $x = 0.1567 + l_p$, where $l_p = 0.17$ cm at the end of discharge (i.e., 3500 s). At the 2*C* rate there is 44% of the original Zn available at the separator at 300 s, about 1.7% at the separator at 600 s and the position at which this zero fraction moves to $l_p = 0.07$ cm.

To understand the physical phenomena leading to these profiles, Fig. 6 shows the corresponding reaction rate distribution in the negative electrode for 1*C* and 2*C* rates as the discharge progresses. There is clearly a *front* that moves from the separator ($x = l_{Ag} + l_{sep} = 0.1567$ cm) towards the anode current collector ($x = l_{Ag} + l_{sep} + l_{Zn} = 0.5567$ cm). As a result, a highly non-uniform reaction distribution, dominated by mass-transfer effects, is observed. Initially a not-so sharp reaction front is restricted to the separator–zinc interface because of high matrix conductivity. Hence, the reaction distribution, shown in Fig. 6 is almost uniform at the beginning of discharge ($t = 0$). As the discharge progresses, the local reaction rate at the separator–zinc interface rises initially to 0.23 and 0.67 A cm^{-3} at 500 and 200 s for 1*C* and 2*C*, respectively. The high reaction rate depletes the active material locally. As a result, the reaction rate shows a maximum after the initial rise corresponding to the region which is rich in the active material. Thus, a reaction front with a distinct peak moves from the separator–zinc interface towards the anode

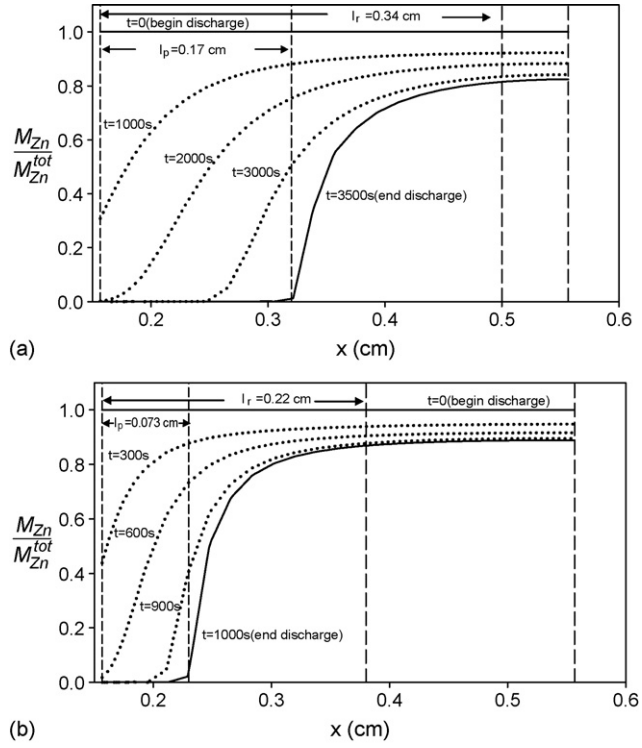

Fig. 5. Distribution profiles of zinc during discharge at various times for (a) 1*C* rate and (b) 2*C* rate. The reaction and penetration depths are also shown. For emphasis, the dashed line on the extreme left of the figures corresponds to the distance $l_{Ag} + l_{sep}$, i.e., the interface between Zn electrode and the separator.

current collector. The curves at 1000 and 1500 s in Fig. 6(a) show the initial stages of the development of this reaction front. At 1500 s the peak of the front has formed and at 2000 s, the development of front is practically complete. Between 2000 and 3500 s (end of discharge) the front moves further to the interior of the zinc electrode consuming more active material and also growing steeper. The movement of the front stops with the end of discharge caused by the local depletion of OH^- ions (see Fig. 3(a)). Similar behavior is shown for the 2*C* rate in Figs. 6(b) and 3(b).

The phenomena behind the formation of the front are interesting. Fig. 3 shows that at any given time, the concentration of OH^- ion decreases along the zinc electrode. However, Fig. 5 shows that at any given time, the fraction of zinc left increases along the positive x direction. Apart from the concentration of OH^- ion and the fraction of zinc left, the anodic overpotential also varies over the zinc electrode. The exponential of this overpotential increases with x (see Eq. (23)), which is consistent with the occurrence of high reaction rate initially at the separator–zinc interface. Eq. (23) suggests that the Butler–Volmer expression involving all these three variables would attain a maximum due to the monotonic behavior of these functions. This explains the existence of a maximum in reaction rate and the movement of the reaction front. In other words, the current density of reaction (3) goes to low values to the left of the maxima since the fraction of zinc approaches zero. Once again it goes to low values to the right of the maxima, since the concentration of OH^- approaches zero. As the reaction front moves through the elec-

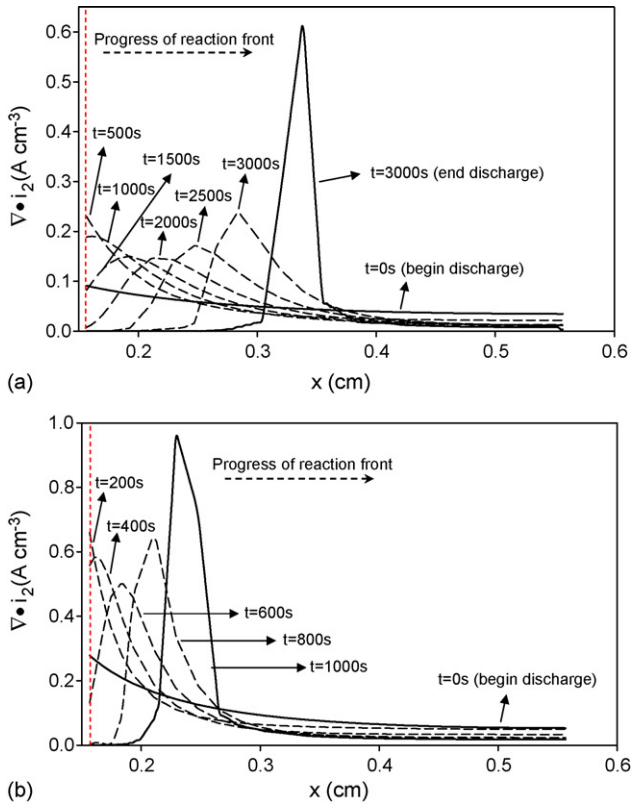

Fig. 6. Reaction distribution in the zinc electrode at various times during discharge for (a) 1*C* and (b) 2*C* rates. Note that a distinct reaction front progresses from the separator–zinc interface into the zinc electrode in both the cases. For emphasis, the dashed line on the extreme left of the figures corresponds to the distance $l_{Ag} + l_{sep}$, i.e., the interface between Zn electrode and the separator.

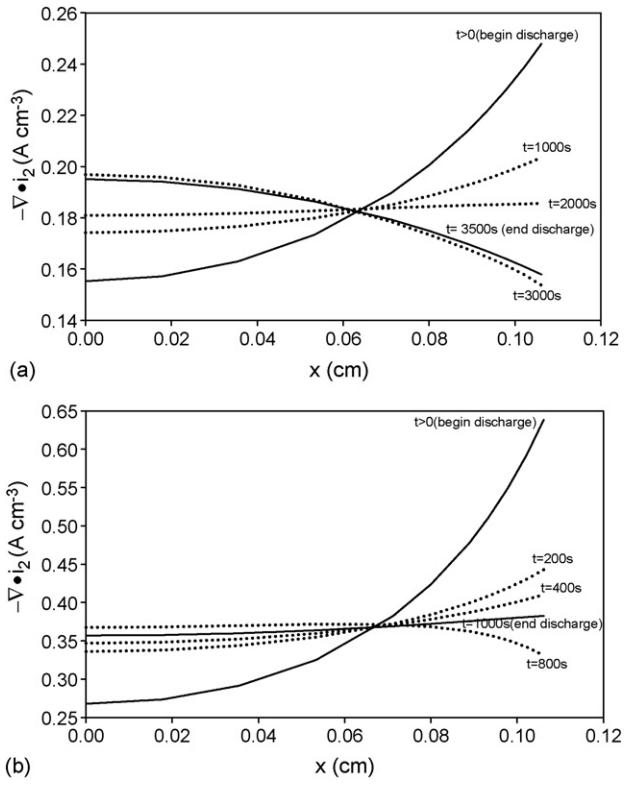

Fig. 7. Reaction distribution in the silver electrode during discharge at various times for (a) 1*C* and (b) 2*C* rates. No reaction front is observed in both the cases. Note that the silver electrode ends at 0.1067 cm.

trode consuming more active material, the overpotential required for the reaction becomes more positive. Fig. 6 also shows that, the value of the maxima increases with time after the front is fully formed. This is because, the rate at which the exponential term involving the overpotential changes is much higher than the rate at which the terms involving concentration or the fraction of active material change. Hence, the value of the maximum reaction rate increases with time as the front moves in the positive x direction.

We define two quantities to understand the distribution of active material in the electrode. Penetration depth (l_p), is defined as the distance from the separator at which the local fraction of zinc left is 0.01 at the end of discharge. For 1*C* rate it is close to 0.15 cm and for 2*C* rate it is 0.07 cm (see Fig. 5). The penetration is a measure of the electrode that was "completely" utilized during discharge and this would correspond to the "dead" region of the cell at the beginning of the charging process. Reaction depth (l_r), is defined as the distance from the separator, where the ratio of the local fraction of Zn left, to the fraction of Zn left at the anode current collector end ($x = l_{Ag} + l_{sep} + l_{Zn} = 0.5567$), is 0.99. From Fig. 5, it may be seen that the reaction depth for 1*C* rate is 0.34 cm and for 2*C* rate it is approximately 0.2 cm. The reaction depth gives an idea about how much of the electrode has been "practically active" during discharge. The difference ($l_p - l_r$) denotes the area where a highly non-uniform distribution of the zinc is observed. A ratio of reaction depth (l_r) to the length of the zinc electrode (l_{Zn}) gives the fraction of area of the electrode active during discharge. It is 85% for 1*C* rate and 50% for 2*C* rate. Penetration depth and reaction depth along with θ_1 (initial mass ratio of zinc to silver in the cell) and θ_2 (initial mass ratio of silver in Ag_2O to silver in AgO) may be used only as "status indicators" of the electrode. Towards the end of discharge the operating conditions start to favor the reverse reactions (charging), and the kinetic resistance is very high. Hence, the cell stops discharging abruptly.

3.3.2. Silver electrode

The corresponding reaction distributions for the positive electrode are presented in Fig. 7. Unlike the zinc electrode, a sharp reaction front is not observed in the silver electrode. The local reaction rate is lower in the positive electrode as can be seen by comparing Figs. 6 and 7. This is because unlike zinc electrode, the reactions at the silver electrode are characterized by products of high electrical conductivity and subsequently a higher matrix current flows in the positive electrode. Apart from this, the production of OH^- ions happens at the positive electrode which increase the conductivity of the electrolyte locally thus facilitating a more uniform consumption of the active material. Although the maximum is not apparent, Fig. 7 shows that the reaction rate distribution is extremely non-uniform at the beginning of discharge and tends to become uniform as the discharge proceeds. At the beginning of discharge, similar to the negative electrode, the reaction rate is high near the silver–separator

interface ($x = l_{Ag} = 0.1067$ cm) and decreases towards the end of discharge. For the 1C rate (see Fig. 7(a)), the rate of reaction is high at the current collector end ($x = 0$) and low at the separator end ($x = l_{Ag} = 0.1067$ cm). However, the rate profile inverts as discharge proceeds and this behavior is observed in the 2C rate. Fig. 7 shows that around 56% SOD (2000 s for 1C rate and 1000 s for 2C rate) the rate profile is uniform and the reaction rate at 2C rate is approximately twice that of 1C. Ref. [38] discusses further the relative ratio of the distribution of these rates.

To facilitate the understanding of the dynamics of the simultaneous reactions in the positive electrode, we define two quantities f, the spatial average of the fraction of current contributed by Ag_2O (i.e., reaction (1)), and g, the spatial average of the dimensionless net rate of production of Ag_2O:

$$f == \frac{1}{l_{Ag}} \int_0^{l_{Ag}} \frac{i_{n_1}}{i_{n_1} + i_{n_2}} \, dx \tag{29}$$

$$g = \frac{1}{l_{Ag}} \int_0^{l_{Ag}} \left(\frac{((-a_{Ag} i_{n_1} s_{Ag_2O,1}/n_1 F) + (-a_{Ag} i_{n_2} s_{Ag_2O,2}/n_2 F))|_t}{((-a_{Ag} i_{n_1} s_{Ag_2O,1}/n_1 F) + (-a_{Ag} i_{n_2} s_{Ag_2O,2}/n_2 F))|_{t=0}} \right) dx \tag{30}$$

The variation of f and g with time are plotted in Fig. 8(a) and (b), respectively. Fig. 8(a) shows that initially f is close to 1 and as discharge proceeds it falls and reaches 0.5. This implies that reaction (1) is much faster than reaction (2) at the beginning of discharge and that slows and becomes equal to the rate of reaction (2). This was observed experimentally by Dirkse [13], who has attributed this to the partial reversibility of reaction (2). The increase in the concentration of OH^- at the cathode drives reaction (2) back. Fig. 8(b) shows that as f approaches 0.5, g approaches 0. At this juncture, the positive electrode may be viewed as having just one overall reaction in which AgO gets converted to Ag without the intermediate Ag_2O. The fraction of silver remaining as Ag_2O is plotted in Fig. 9. The profiles for the 1C and 2C rates are the same in Fig. 9 and it is interesting to note that, the Ag_2O becomes locally depleted at 22.2% SOD which is after 800s for 1C rate and after 400 s for 2C rate (see Fig. 8). This is again is a result of the overall rate being set by the reaction (2), so that as Ag_2O is produced by reactions (2) and (1) consumes it immediately. The local depletion of Ag_2O happening much earlier than the end of discharge is also consistent with the cell-voltage behavior circled in Fig. 2. The exchange current densities i_{01} and i_{02} of reactions (1) and (2) have a significant influence on the times at which the depletion of occurs. This is discussed in the following section.

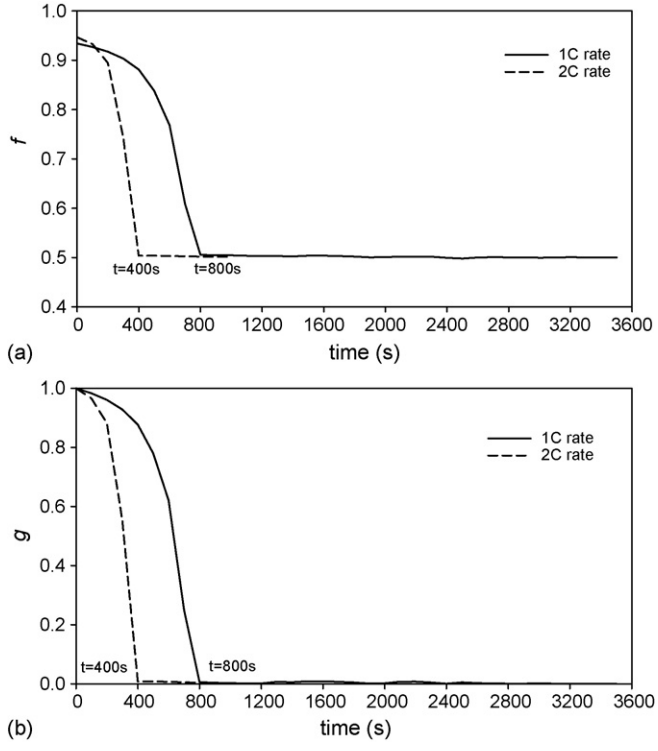

Fig. 8. Variation of (a) average rate of reaction (1) (normalized) and (b) average rate of production of Ag_2O (normalized) with time in the silver electrode. Note that both 1C and 2C rates are featured in the same graph. See Fig. 2, for comparison.

3.4. Effect of exchange current density

Because the kinetic parameters are difficult to measure in this system and not reported, we consider perturbations from those used above. Specifically, we are interested in the interaction of the reactions (1) and (2), and how the kinetic parameters of those reactions affect the behavior of the time-dependent cell voltage. Similarly the movement of the front in the zinc electrode also is influenced by the kinetic parameters of the system. Two exchange current densities, namely i_{01} and i_{03} were varied here while i_{02} was kept constant. Fig. 10(a) and (b) shows the effect of i_{01} and i_{03} exchange currents densities on the cell-voltage behavior. Three values of i_{01}: 2×10^{-3}, 2×10^{-4}, and 2×10^{-5} A cm^{-2}, were used to study the behavior of the cell (see Table 3, for values of parameters). i_{01} has a pronounced effect on the cell voltage. Fig. 10(a) shows that, the OCV drops by approximately 0.05 V for an order of magnitude drop in i_{01}. A comparison between curves 1 and 4 in Fig. 10(a) shows that the

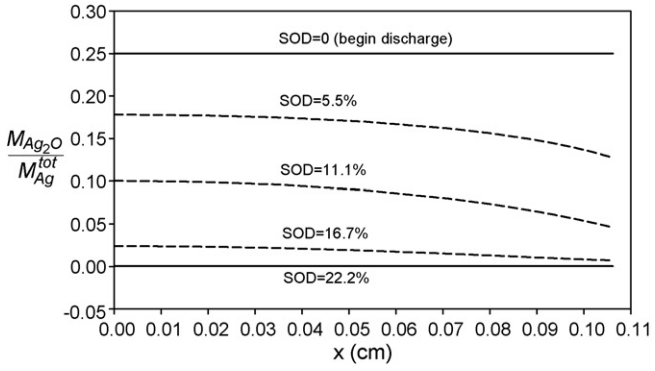

Fig. 9. Profiles of distribution of Ag_2O over the silver electrode during discharge. At a given SOD, the profiles obtained at 1C and 2C rates do not show a significant difference between them. Note that the silver electrode ends at 0.1067 cm.

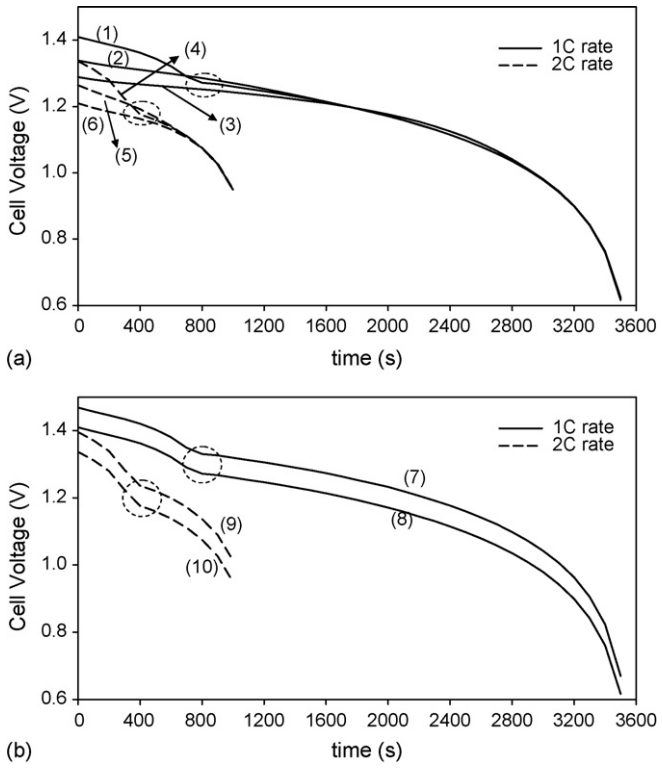

Fig. 10. Effect of exchange current density (a) i_{01} and (b) i_{03} on cell performance. For curves (1)–(10), see Table 3, for the parameter values. The encircled regions indicate the change in the behavior of the curves at $t = 800$ and 400 s for 1C and 2C rate discharges, respectively. See Fig. 2, for comparison.

model has captured the sharp fall in the cell voltage. This agrees well with the experimentally measured value of 1.45 V for the initial cell voltage reported by Moden [36] for 1C rate. In the low rate studies (0.1C), a stable potential of 1.55 V was predicted by the model (not shown), which once again agrees very well with the experimentally observed value of 1.59 V per cell of Moden [36]. Thus, silver oxide materials with a high exchange current density for reaction (1) are bound to yield higher cell voltage and also withstand higher rates of discharge. It is also notable that for a value of 2×10^{-3} A cm^{-2} for i_{01}, a considerable decrease in the slope happens for both 1C and 2C rates at 800 and 400 s, respectively (marked by dotted circles in Figs. 2 and 10). This change in curve behavior is consistent with the local depletion of Ag_2O as discussed in the previous section and also Fig. 2. However, at a lower value of i_{01}, the depletion of Ag_2O is delayed and happens at a higher SOD. For example, for i_{01} values 2×10^{-4} and 2×10^{-5} A cm^{-2}, the SOD at which depletion of Ag_2O happens are 66.7 and 88.9%, respectively. A lower value of i_{01} reduces the rate of reaction (1) and hence a slower depletion of Ag_2O. At an i_{01} value of 2×10^{-5} A cm^{-2} the rate of reaction (1) is slowed down greatly that an initial increase in Ag_2O due to the contribution of reaction (2) is observed. Thus, Ag_2O reaches a maximum concentration and falls off thereafter due to the increased consumption by reaction (1). Further details about profiles of Ag_2O may be obtained from Ref. [38].

The effect of i_{03} on cell voltage is similar to i_{01}. Fig. 10(b) shows that the cell voltage drops by 0.05 V for an order of magnitude drop in i_{03}. A higher exchange current density thus would

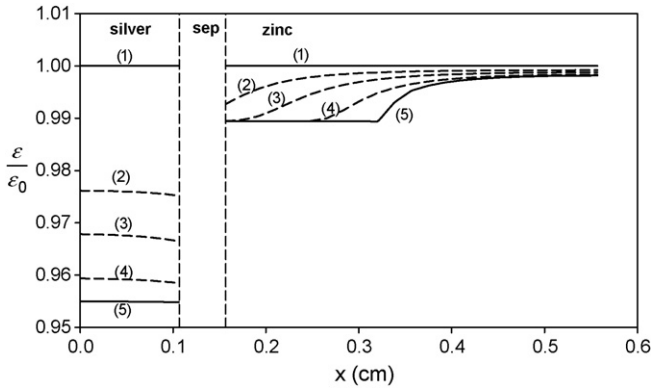

Fig. 11. Typical porosity distribution profiles in a silver–zinc cell during discharge at various SOD: (1) 0%, (2) 27.7%, (3) 55.4%, (4) 83.3%, and (5) 97.2%. At a given SOD, the profiles obtained at 1C and 2C rates do not show a significant difference between them. However, MSOD for 2C rate is 55.4%.

lead to a higher cell voltage. A value of 1.75×10^{-4} A cm^{-2} did not allow the cell to discharge since kinetic resistance of the cell became high. Both the exchange current densities have almost no effect on MSOD. This is because under normal operating conditions with high rate discharges the system is usually under mass-transfer control. It is the local non-availability of the OH^- ions that leads to the abrupt end of discharge thereby lowering MSOD.

3.5. Porosity distribution

Fig. 11 shows the variation of porosity over the electrode at different times at the 1C rate. The y axis of the plot is the ratio of instantaneous porosity to the initial porosity in the respective regions. The separator porosity is a constant since no reaction takes place in that region and no clogging of the separator by reaction solids is assumed. The porosity of both electrodes do not vary appreciably during discharge. This may obviate the need to include the porosity equations during a solution of the three-dimensional equations. Apart from reducing the bandwidth of the system of equations, it also attenuates the difficulty in solving the concentration equations since a constant porosity reduces the non-linearity to a good extent.

3.6. Temperature rise and profiles

The present model includes a thermal energy equation (refer Eq. (25)), accounting for the reversible, kinetic, and joule heating terms involved in heating of a cell during discharge. Since, the conductivities of the materials in a silver–zinc cell are high, a low discharge rate (i.e., <1C) does not effect a local temperature rise and even at the 2C rate for a single cell, the temperature at a given instant of time does not vary appreciably over x. Hence, a plot of average temperature rise versus time would be sufficient to understand the thermal behavior of the system. By average temperature rise, we mean:

$$T_{\text{avg}}(t) - T_0 = \frac{1}{l_{\text{Ag}} + l_{\text{sep}} + l_{\text{Zn}}} \int_0^{l_{\text{Ag}}+l_{\text{sep}}+l_{\text{Zn}}} (T(x,t) - T_0)\,\mathrm{d}x \tag{31}$$

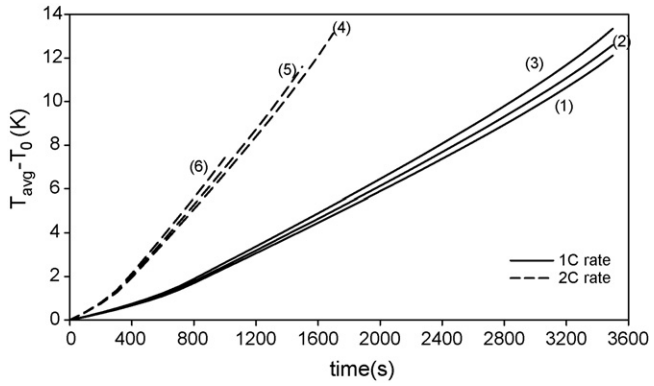

Fig. 12. Effect of initial concentration (%KOH) on average temperature rise. For curves (1)–(6), see Table 3, for the parameter values.

The effect of initial concentration, C_0, on the average temperature rise is shown in Fig. 12. Concentration affects the average temperature-rise by affecting the discharge time and the thermal and electrical properties of the electrolyte. Thus, a longer discharge time implies a longer heating and a higher maximum temperature although the average temperature decreases with an increase in initial concentration. Moden [36] observed an average temperature rise of 0.22 and 0.54 K min^{-1} for 1C and 2C rate of discharge, respectively. An inspection of Fig. 12 shows that the average temperature-rise reaches approximately 14 K at 1C rate at end of discharge (∼0.23 K min^{-1}) and shows 0.48 K min^{-1} for the 2C rate. This difference between the observed and predicted rise could be a result of different external boundary conditions or kinetic parameters.

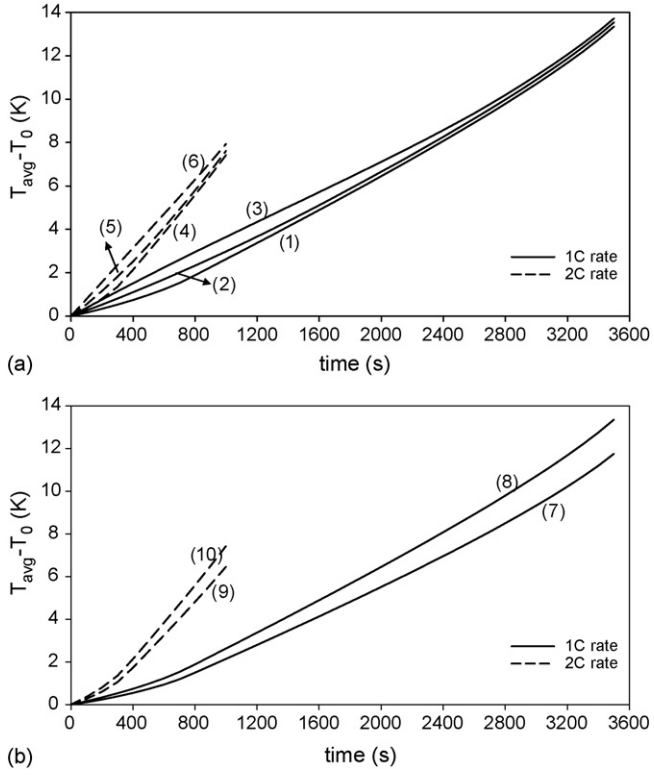

Fig. 13. Effect of exchange current density (a) i_{01} and (b) i_{03} on average temperature rise. For curves (1)–(10), see Table 3, for the parameter values.

Fig. 13 shows that, at 2C, decreasing i_{01} two orders of magnitude removes the changes in the initial slope so that the rise is more linear, however the final temperature difference is insignificant. On the other hand, a larger value of i_{03} lowers the average temperature rise in the cell.

4. Conclusions

A mathematical model has been developed and used to study the time-dependent and position-dependent performance and thermal behavior of the silver–zinc cell during discharge. Species and reaction distributions have been predicted. The model predicts that the discharge may reach an abrupt end at high discharge rates, because of mass transfer limitations. The simultaneous reactions in the positive electrode influence the behavior of the cell voltage–time curve considerably. Porosity variations were not found to be important. The temperature rise was predicted and found to be agreeable with reported experimental values. A high concentration of the alkali electrolyte and well-prepared electrodes with high exchange current densities and low tortuosity could increase the capacity utilization.

Acknowledgement

The authors gratefully acknowledge support for this work from ONR grant N00014-98-1-0554.

References

[1] A.P. Karpinski, B. Makovetski, S.J. Russell, J.R. Serenyi, D.C. Williams, J. Power Sources 80 (1999) 53–60.
[2] B. Hariprakash, S.K. Martha, A.K. Shukla, J. Power Sources 117 (2003) 242–248.
[3] O. Hasvold, N. Storkersen, J. Power Sources 96 (2001) 252.
[4] A. Himy, Silver–Zinc Battery—Phenomena and Design Principles, 1st ed., Vantage Press, New York, 1986.
[5] P. Suresh, D.H. Nagaraju, A.K. Shukla, N. Munichandraiah, Electrochim. Acta 50 (2005) 3262–3272.
[6] H.L. Lewis, T. Danko, A. Himy, W. Johnson, J. Power Sources 80 (1999) 61–65.
[7] D.F. Smith, C. Brown, J. Power Sources 96 (2001) 121–127.
[8] S. Dallek, W.A. West, B.F. Larrick, J. Electrochem. Soc. 133 (1986) 2451–2454.
[9] A.J. Salkind, R.W. Freeman, J.J. Weckesser, W.A. West, S. Dallek, J. Electrochem. Soc. 135 (1988) 1882–1887.
[10] J.A. Gucinski, M. Slack, J. Power Sources 96 (2001) 246–258.
[11] W.J. Hamer, D.N. Craig, J. Electrochem. Soc. 103 (1956) C200.
[12] W.J. Hamer, D.N. Craig, J. Electrochem. Soc. 104 (1957) 206–211.
[13] T.P. Dirkse, J. Electrochem. Soc. 106 (1959) 453–457.
[14] C.P. Wales, J. Burbank, J. Electrochem. Soc. 106 (1959) 885–890.
[15] C.P. Wales, J. Burbank, J. Electrochem. Soc. 111 (1964) C182.
[16] T.P. Dirkse, J. Electrochem. Soc. 109 (1962) 173–177.
[17] E.G. Gagnon, L.G. Austin, J. Electrochem. Soc. 119 (1972) 807.
[18] F.R. Mclarnon, E.J. Cairns, J. Electrochem. Soc. 138 (1991) 645–664.
[19] K.W. Choi, D.N. Bennion, J. Newman, J. Electrochem. Soc. 123 (1976) 1616–1627.
[20] K.W. Choi, D. Hamby, D.N. Bennion, J. Newman, J. Electrochem. Soc. 123 (1976) 1628–1637.
[21] D. Hamby, J. Wirkkala, J. Electrochem. Soc. 125 (1978) 1020–1026.
[22] W.G. Sunu, J. Electrochem. Soc. 127 (1980) 2007–2016.

[23] W.G. Sunu, D.N. Bennion, J. Electrochem. Soc. 127 (1980) 2017–2025.
[24] J. Skelton, R. Serenyi, J. Power Sources 65 (1997) 39–45.
[25] J.S. Chen, H.Y. Cheh, J. Electrochem. Soc. 140 (1993) 1205–1213.
[26] J.S. Newman, C.W. Tobias, J. Electrochem. Soc. 109 (1962) 1183–1191.
[27] J. Newman, W. Tiedemann, AlChE J. 21 (1975) 25–41.
[28] S.L. Blanton, J.W. Weidner, J.W. Van Zee, Proceedings of the Douglas N. Bennion Memorial Symposium, The Electrochemical Society Inc., 1994, pp. 208–228.
[29] K.W. Choi, N.P. Yao, J. Electrochem. Soc. 125 (1978) 1011–1019.
[30] K.W. Choi, N.P. Yao, J. Electrochem. Soc. 126 (1979) 1321–1328.
[31] H.F. Gibbard, J. Electrochem. Soc. 125 (1978) 353–358.
[32] M.J. Lampinen, M. Fomino, J. Electrochem. Soc. 140 (1993) 3537–3546.
[33] D. Bernardi, E. Pawlikowski, J. Newman, J. Electrochem. Soc. 132 (1985) 5–12.
[34] C.R. Pals, J. Newman, J. Electrochem. Soc. 142 (1995) 3274–3281.
[35] C.R. Pals, J. Newman, J. Electrochem. Soc. 142 (1995) 3282–3288.
[36] J.R. Moden, Personal Communication and Unpublished Lecture notes "Chemical Engineering 'Art and Science' as Applied to Zinc–Silver Oxide Batteries", University of South Carolina, 1996.
[37] J.S. Newman, Electrochemical Systems, 2nd ed., Prentice-Hall, Englewood Cliffs, 1991.
[38] M. Venkatraman, Chemical Engineering, Ph.D. Thesis, University of South Carolina, Columbia, 2006.
[39] K.W. Choi, D. Hamby, D.N. Bennion, J. Newman, J. Electrochem. Soc. 122 (1975) C243.
[40] FEMLAB 2.1, COMSOL Inc., http://www.comsol.com.
[41] A. Himy, Silver–Zinc Battery—Best Practice, Facts and Reflections, 1st ed., Vantage Press, New York, 1985.
[42] E.J. Podlaha, H.Y. Cheh, J. Electrochem. Soc. 141 (1994) 15–27.
[43] D.R. Lide (Ed.), CRC Handbook of Chemistry and Physics, CRC, 2006.